ELSEVIER

Journal of Structural Geology 28 (2006) 957–971

JOURNAL OF STRUCTURAL GEOLOGY

www.elsevier.com/locate/jsg

Embedding stress difference in parameter space for stress tensor inversion

Katsushi Sato *, Atsushi Yamaji

Division of Earth and Planetary Sciences, Graduate School of Science, Kyoto University, Kyoto 606-8502, Japan

Abstract

This paper proposes a rearrangement of Fry's sigma-space which has translated stress tensor inversion into a concise geometric problem. The kernel of our modification is in the normalisations of tensor invariants and in the adoption of weighting factors used in the studies of crystal plasticity. After describing a fault-slip datum as a strain tensor, we mapped both stress and strain tensors onto the modified parameter space. There are two main benefits. First, the geometry is simplified. The points representing normalised tensors are located on the five-dimensional unit sphere and their relative arrangement is independent from the coordinate selection in physical space. Second, the Euclidean metric of the space was equated to the so-called stress difference, a useful measure of difference between normalised stress tensors. This metric led us to a straightforward method for quantifying the confidence region of stress tensor deduced through inversion.

Keywords: Sigma-space; Stress difference; Stress tensor inversion; Fault-slip analysis; Error estimation

1. Introduction

Palaeostress analysis is the key to the elucidation of tectonic events. A number of inversion techniques have been devised for reconstructing stress tensors from fault-slip data (e.g. Carey and Brunier, 1974; Angelier, 1979; Etchecopar et al., 1981; Gephart and Forsyth, 1984; Simón-Gómez, 1986; Nemcok and Lisle, 1995; Yamaji, 2000; Shan et al., 2003). The latter five methods attempt to separate multiple stress states from heterogeneous data. Recently, Fry (1999, 2001) has proposed a geometrical interpretation of the inverse problem using a six-dimensional component-wise parameter space of stress tensor, which was termed 'σ-space'. He clearly divided the problem into linear and non-linear parts and specified the constraint on stress tensor from a single fault-slip datum as a region in σ-space.

The purpose of this study is to assess the significance of the metric in the parameter space. Our formulation equates the Euclidean distance to the stress difference (Orife and Lisle, 2003), which is a well-defined and convenient measure of difference between normalised stress tensors. This metric enables us to quantify the confidence region not of principal orientations, but of the stress tensor itself. Furthermore, our modification simplifies the inverse problem into the geometry on the five-dimensional unit sphere. The admissible region of stress tensor constrained by a fault was clarified in a normalised form.

The statistical reliability of the solution of the stress tensor inversion has been intensively investigated with respect to the effect of errors, biases and heterogeneity in the fault-slip data (e.g. Etchecopar et al., 1981; Gephart and Forsyth, 1984; Choi et al., 1996; Albarello, 2000; Yamaji, 2003; Xu, 2004). There is a serious problem in estimating and even in defining the variance of a tensor quantity. Orife and Lisle (2003) have pointed out that any assessment of stress tensor should not be based solely on orientations, since their stabilities depend on the shape of stress ellipsoid or stress ratio and vice versa. Yamaji et al. (2005) used the mean stress difference to estimate the spread of stress tensors as a scalar value. The present article aims to express the confidence region by a covariance matrix including the anisotropy in the parameter space.

The next section provides the definition and mathematical foundations of the reshaped parameter space. Sections 3 and 4 convert the stress tensor and fault-slip data into points on the hypersphere, respectively. In Section 5, the geometrical interpretation of stress tensor inversion (Fry, 1999, 2001) is found to be valid for our parameter space with newly added features. The numerical experiments in Section 6 confirm the theoretical advantages of the new formulation. The method of error estimation is presented in Section 7. The notation used in this paper is listed in Table 1.

* Corresponding author. Tel.: +81 75 753 7531 (ext. 4173); fax: +81 75 753 4189.

E-mail address: k_sato@kueps.kyoto-u.ac.jp (K. Sato).

0191-8141/$ - see front matter © 2006 Published by Elsevier Ltd.
doi:10.1016/j.jsg.2006.03.004

Table 1
List of symbols in alphabetical order

Symbol	Description	Reference
$\hat{b}$	The direction normal to both $\hat{n}$ and $\hat{v}$	Figs. 2 and 3
D	Stress difference	Eqs. (17) and (D.2)
$d\vec{\sigma}^{[4]}$	$\vec{\sigma}-\vec{\mu}$ projected onto P^4_μ	Eq. (50)
$\mathbf{E}$	Strain tensor	Eq. (21)
$\mathbf{E}'$	Virtual strain tensor	Eq. (23)
E_1, E_2, E_3	Principal strains	Eq. (25)
$\mathbf{F}$	Deformation gradient tensor	Eq. (19)
$\vec{\mathcal{F}}_5$	Map from symmetric and deviatoric tensor to 5-D vector	Eq. (6)
$\vec{\mathcal{F}}_6$	Map from symmetric tensor to 6-D vector	Eq. (1)
$\mathbf{G}$	Displacement gradient tensor	Eq. (19)
$\mathbf{I}$	3-D unit tensor	
J_I	First invariant (trace)	Eq. (2)
J_II	Second invariant	Eq. (3)
J_III	Third invariant (determinant)	
M	Number of bootstrap iteration	Section 7.1
n	Factor specifying confidence level	Eq. (51)
$\hat{n}$	Fault normal	Figs. 2 and 3
N	Number of fault	
P^4_μ	4-D plane normal to $\vec{\mu}$	Fig. 9
P^5_π	5-D plane normal to $\vec{\pi}$	Eq. (4)
$\mathbf{Q}$	6-D rotation tensor	Eq. (A.1)
$\mathbf{S}$	Stress tensor, tension being positive	Section 3
S_1, S_2, S_3	Principal stresses, tension being positive	
S_5	5-D unit sphere	Fig. 1
S_6	6-D unit sphere	Eq. (5)
$\boldsymbol{t}$	Traction vector	Fig. 3
$\hat{v}$	Slip direction	Figs. 2 and 3
$\mathbf{V}^{[4]}$	4-D covariance matrix	Eq. (50)
W	Work done on a rock mass	Eq. (36)
W'	Virtual work done on a rock mass	Eq. (38)
$\mathbf{X}$	A symmetric tensor	Section 2
γ	Engineering shear strain	Eqs. (19)–(21)
γ'	Engineering virtual shear strain	Eqs. (22) and (23)
$\boldsymbol{\Delta}$	Angular misfit	Eqs. (45) and (46)
$\vec{\varepsilon}, \vec{\varepsilon}^{[5]}$	5-D ε-vector	Eq. (31)
$\vec{\varepsilon}', \vec{\varepsilon}'^{[5]}$	5-D ε'-vector	Eq. (32)
$\vec{\varepsilon}^{[6]}$	6-D ε-vector	Eq. (29)
$\vec{\varepsilon}'^{[6]}$	6-D ε'-vector	Eq. (30)
$\vec{\mu}$	5-D mean σ -vector	Eq. (49)
$\vec{\pi}$	Unit normal of P^5_π	Fig. 1
ρ	Normalising factor	Eq. (49)
σ	Stress tensor, compression being positive	
$\sigma_1, \sigma_2, \sigma_3$	Principal stresses, compression being positive	
$\vec{\sigma}, \vec{\sigma}^{[5]}$	5-D σ-vector	Eq. (15)
$\vec{\sigma}^{[6]}$	6-D σ-vector	Eq. (14)
$\boldsymbol{\tau}$	Resolved shear stress on a fault surface	Fig. 3
τ_oct	Octahedral shear stress	Appendix D
Φ	Stress ratio	Eq. (C.1)

2. Parameter space for tensor quantities

2.1. Definition

For the purpose of dealing with stress and strain tensors equivalently, the parameter space was defined in a generalised form for symmetric tensor quantities. We use the term 'tensor' to denote a second-rank tensor (matrix).

The parameter space is the six-dimensional Euclidean space. We define a map, $\vec{\mathcal{F}}_6$, which associates an arbitrary symmetric tensor $\mathbf{X}=\{X_{ij}\}$ with a six-dimensional vector:

$$\vec{\mathcal{F}}_6(X) \equiv \left(\frac{X_{11}}{\sqrt{2}},\ \frac{X_{22}}{\sqrt{2}},\ \frac{X_{33}}{\sqrt{2}},\ X_{23},\ X_{31},\ X_{12}\right)^\mathrm{T}. \tag{1}$$

The superscript T represents the transpose of a vector or tensor. We denote high-dimensional vectors with arrows, while vectors and tensors in physical space are indicated by bold letters.

The difference between $\vec{\mathcal{F}}_6$ and the definition of σ-space (Fry, 1999, 2001) is in the diagonal components of $\mathbf{X}$ divided by $\sqrt{2}$. Such weight factors have been used in the theories of plasticity (e.g. Takahashi et al., 1990; Levitas and Preston, 2002). They multiply the off-diagonal components by $\sqrt{2}$ instead of dividing the diagonal components.

2.2. Normalisations and their geometric meanings

In this paper, tensors are frequently normalised by two conditions:

$$J_\mathrm{I}(\mathbf{X}) \equiv X_{11}+X_{22}+X_{33}=0, \tag{2}$$

$$J_\mathrm{II}(\mathbf{X}) \equiv \frac{1}{2}\left(X_{11}^2+X_{22}^2+X_{33}^2\right)+X_{23}^2+X_{31}^2+X_{12}^2=1, \tag{3}$$

where J_I and J_II are the first and second invariants of the tensor (Fung, 1965, p. 80), respectively. The first normalisation makes a tensor deviatoric. Note that the definition of the second invariant in Eq. (3) is applicable only to deviatoric tensors.

These normalisations have geometric meanings. Let $\vec{x}=(x_1,x_2,\ldots,x_6)^\mathrm{T}$ be the vector $\vec{\mathcal{F}}_6(\mathbf{X})$ in Eq. (1), then we can rewrite Eqs. (2) and (3) as

$$x_1+x_2+x_3=0, \tag{4}$$

$$x_1^2+x_2^2+x_3^2+x_4^2+x_5^2+x_6^2=1. \tag{5}$$

Eq. (4) represents a five-dimensional plane through the origin of the parameter space and perpendicular to $(1, 1, 1, 0, 0, 0)^\mathrm{T}$. We use the symbol P^5_π for this plane and $\vec{\pi}=\left(\frac{1}{\sqrt{3}},\ \frac{1}{\sqrt{3}},\ \frac{1}{\sqrt{3}},\ 0,\ 0,\ 0\right)^\mathrm{T}$ for the unit vector parallel to the normal. On the other hand, Eq. (5) represents the six-dimensional unit sphere, which we refer to as S_6. The normalised tensors are represented by points on the intersection of P^5_π and S_6, which is the five-dimensional unit sphere (Fig. 1). We use the symbol S_5 for this hypersphere.

Since the vector $\vec{\mathcal{F}}_6(\mathbf{X})$ has the end point on S_5, it can be expressed also as a five-dimensional vector through a simple coordinate rotation (Appendix A):

$$\vec{\mathcal{F}}_5(\mathbf{X}) \equiv \left(-\left(\frac{1}{2\sqrt{2}}+\frac{1}{2\sqrt{6}}\right)X_{11}+\left(\frac{1}{2\sqrt{2}}-\frac{1}{2\sqrt{6}}\right)X_{22}+\frac{1}{\sqrt{6}}X_{33},\ \left(\frac{1}{2\sqrt{2}}-\frac{1}{2\sqrt{6}}\right)X_{11}-\left(\frac{1}{2\sqrt{2}}+\frac{1}{2\sqrt{6}}\right)X_{22}+\frac{1}{\sqrt{6}}X_{33},\ X_{23}, X_{31}, X_{12}\right)^\mathrm{T}, \tag{6}$$

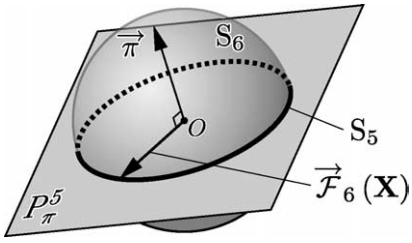

Fig. 1. Schematic figure of six-dimensional parameter space. A symmetric tensor $\mathbf{X}$ is normalised by $J_{\mathrm{I}}=0$ and $J_{\mathrm{II}}=1$. The vector $\vec{\mathcal{F}}_6(\mathbf{X})$ lies on the unit sphere S_6 and the plane P^5_π perpendicular to $\vec{\pi}\equiv\left(\frac{1}{\sqrt{3}},\frac{1}{\sqrt{3}},\frac{1}{\sqrt{3}},0,0,0\right)^{\mathrm{T}}$. Therefore, the existence region of $\vec{\mathcal{F}}_6(\mathbf{X})$ is the five-dimensional unit sphere S_5, which is shown as a bold great circle in this figure.

where the second normalisation (Eq. (3)) corresponds to

$$\left|\vec{\mathcal{F}}_5(\mathbf{X})\right|=1. \tag{7}$$

Note that $\vec{\mathcal{F}}_5(\mathbf{X})$ and $\vec{\mathcal{F}}_6(\mathbf{X})$ indicate the same object, and especially:

$$\left|\vec{\mathcal{F}}_5(\mathbf{X}_{\mathrm{A}})-\vec{\mathcal{F}}_5(\mathbf{X}_{\mathrm{B}})\right|=\left|\vec{\mathcal{F}}_6(\mathbf{X}_{\mathrm{A}})-\vec{F}_6(\mathbf{X}_{\mathrm{B}})\right|, \tag{8}$$

$$\vec{\mathcal{F}}_5(\mathbf{X}_{\mathrm{A}})\cdot\vec{\mathcal{F}}_5(\mathbf{X}_{\mathrm{B}})=\vec{\mathcal{F}}_6(\mathbf{X}_{\mathrm{A}})\cdot\vec{\mathcal{F}}_6(\mathbf{X}_{\mathrm{B}}), \tag{9}$$

for any two symmetric matrices $\mathbf{X}_{\mathrm{A}}$ and $\mathbf{X}_{\mathrm{B}}$.

2.3. Metric

The Euclidean metric in our parameter space is given by the square root of the second invariant of the tensor (see Appendix B for derivation). For any two symmetric and deviatoric tensors $\mathbf{X}_{\mathrm{A}}$ and $\mathbf{X}_{\mathrm{B}}$:

$$\left|\vec{\mathcal{F}}_5(\mathbf{X}_{\mathrm{A}})-\vec{\mathcal{F}}_5(\mathbf{X}_{\mathrm{B}})\right|=\sqrt{J_{11}(\mathbf{X}_{\mathrm{D}})}, \tag{10}$$

where $\mathbf{X}_{\mathrm{D}}=\mathbf{X}_{\mathrm{A}}-\mathbf{X}_{\mathrm{B}}$. Furthermore, by setting $\mathbf{X}_{\mathrm{B}}=0$ in Eq. (10), we have

$$\left|\vec{\mathcal{F}}_5(\mathbf{X})\right|=\sqrt{J_{11}(\mathbf{X})}, \tag{11}$$

for any symmetric and deviatoric tensor $\mathbf{X}$. Any coordinate rotation in physical space does not affect the metric in the parameter space owing to the nature of invariant.

3. Mapping stress tensor onto parameter space

3.1. σ-vector

Except for Sections 6 and 7 and Appendices A and B, this paper uses the sign convention of continuum mechanics, i.e. tension is positive for the stress tensor denoted by $\mathbf{S}=\{S_{ij}\}$ (i, $j=1, 2, 3$). A stress tensor, which is assumed to be symmetric, has six independent components. However, the stress tensor inversion can constrain only four degrees of freedom (see Section 5.1 for the reason for this reduction). The normalised stress tensor, the so-called 'reduced stress tensor' (Angelier, 1984), can be described by principal orientations and a stress ratio (Eq. (C.1)).

Since two normalisations can be freely chosen, we adopt

$$J_{\mathrm{I}}(\mathbf{S})=0,\quad J_{\mathrm{II}}(\mathbf{S})=1. \tag{12}$$

A practical form of these normalisations is presented in Appendix C. The first normalisation was also used by Fry (1999). However, he adopted the constraint:

$$S_{11}^2+S_{22}^2+S_{33}^2+S_{23}^2+S_{31}^2+S_{12}^2=1, \tag{13}$$

instead of the second one. The left-hand side of Eq. (13) is not an invariant of the stress tensor, namely, the principal values of normalised stress tensor depend on the coordinate system. Our normalisations avoid this problem.

According to Eq. (1), a reduced stress tensor is mapped onto the parameter space:

$$\vec{\sigma}^{[6]}\equiv\vec{\mathcal{F}}_6(\mathbf{S})=\left(\frac{S_{11}}{\sqrt{2}},\ \frac{S_{22}}{\sqrt{2}},\ \frac{S_{33}}{\sqrt{2}},\ S_{23},\ S_{31},\ S_{12}\right)^{\mathrm{T}}, \tag{14}$$

where the vector $\vec{\sigma}^{[6]}$ was termed 'σ-vector', following Fry (1999). Since the normalisations (Eq. (12)) are identical to those in Section 2.2, we have the five-dimensional expression of the σ-vector:

$$\vec{\sigma}^{[5]}\equiv\vec{\mathcal{F}}_5(\mathbf{S})=\left(-\left(\frac{1}{2\sqrt{2}}+\frac{1}{2\sqrt{6}}\right)S_{11}+\left(\frac{1}{2\sqrt{2}}-\frac{1}{2\sqrt{6}}\right)S_{22}+\frac{1}{\sqrt{6}}S_{33},\right.$$
$$\left(\frac{1}{2\sqrt{2}}-\frac{1}{2\sqrt{6}}\right)S_{11}-\left(\frac{1}{2\sqrt{2}}+\frac{1}{2\sqrt{6}}\right)S_{22}+\frac{1}{\sqrt{6}}S_{33},$$
$$\left.S_{23},\ S_{31},\ S_{12}\right)^{\mathrm{T}}, \tag{15}$$

Its existence region is the five-dimensional unit sphere S_5:

$$\left|\vec{\sigma}^{[5]}\right|=1. \tag{16}$$

3.2. Embedded stress difference

The metric in the parameter space has a significant physical meaning, the stress difference D (Orife and Lisle, 2003). We found an equivalent formulation of stress difference to the original definition (Appendix D):

$$D(\mathbf{S}_{\mathrm{A}},\ \mathbf{S}_{\mathrm{B}})\equiv\sqrt{J_{11}(\mathbf{S}_{\mathrm{D}})}, \tag{17}$$

where both $\mathbf{S}_{\mathrm{A}}$ and $\mathbf{S}_{\mathrm{B}}$ are normalised by Eq. (12) and $\mathbf{S}_{\mathrm{D}}=\mathbf{S}_{\mathrm{A}}-\mathbf{S}_{\mathrm{B}}$ is called the 'difference tensor'. The stress difference is a function of $\mathbf{S}_{\mathrm{A}}$ and $\mathbf{S}_{\mathrm{B}}$ and its value ranges from 0 to 2. $D=0$ for identical tensors, while $D=2$ when the two tensors are 'negative tensors' to each other ($\mathbf{S}_{\mathrm{A}}=-\mathbf{S}_{\mathrm{B}}$).

Combining Eqs. (10) and (17), we have

$$\left|\vec{\mathcal{F}}_5(\mathbf{S}_{\mathrm{A}})-\vec{\mathcal{F}}_5(\mathbf{S}_{\mathrm{B}})\right|=D(\mathbf{S}_{\mathrm{A}},\ \mathbf{S}_{\mathrm{B}}). \tag{18}$$

The stress difference can be measured as the Euclidean distance in the parameter space. When we have some scattered points indicated by σ-vectors on S_5, they are separated according to the stress differences between corresponding

reduced stress tensors. For instance, take a stress tensor and its negative tensor represented by $\vec{\sigma}^{[5]}$ and $-\vec{\sigma}^{[5]}$, respectively. They are antipodal points and their Euclidean distance equals two, which is the diameter of the unit sphere S_5. This value is expectedly the maximum stress difference $D=2$.

4. Mapping fault-slip data onto parameter space

4.1. Introduction of strain tensor

This subsection introduces a strain tensor as an equivalent of a fault-slip datum. A datum can be described by the fault normal $\hat{n}$ pointing outward from the footwall block and the slip direction of the block $\hat{v}$ (Fig. 2a). We utilise another vector $\hat{b}$ on the fault plane at right angles to $\hat{v}$. Hereafter, bold letters with hats denote unit vectors in physical space.

We assume the strain caused by a fault to be simple shear (Fig. 2b). When we take the vectors $\hat{v}$, $\hat{b}$ and $\hat{n}$ as Cartesian coordinate axes, which we call 'fault coordinate system', the deformation gradient tensor $\mathbf{F}$ (e.g. Khan and Huang, 1995, p. 52) and the displacement gradient tensor $\mathbf{G}$ for the simple shear are

$$\mathbf{F}=\begin{pmatrix}1&0&-\gamma\\0&1&0\\0&0&1\end{pmatrix},\quad \mathbf{G}=\mathbf{F}-\mathbf{I}=\begin{pmatrix}0&0&-\gamma\\0&0&0\\0&0&0\end{pmatrix}, \tag{19}$$

where γ is the engineering shear strain, and $\mathbf{I}$ is the unit tensor. Accordingly, Cauchy's strain tensor (e.g. Fung, 1965, p. 94) is

$$\mathbf{E}=\frac{1}{2}\left(\mathbf{G}+\mathbf{G}^{\mathrm{T}}\right)=-\frac{\gamma}{2}\begin{pmatrix}0&0&1\\0&0&0\\1&0&0\end{pmatrix}, \tag{20}$$

where extension is positive. In general coordinate system:

$$\mathbf{E}=-\frac{\gamma}{2}\left(\hat{v}\,\hat{b}\,\hat{n}\right)\begin{pmatrix}0&0&1\\0&0&0\\1&0&0\end{pmatrix}\left(\hat{v}\,\hat{b}\,\hat{n}\right)^{\mathrm{T}}$$

$$=-\frac{\gamma}{2}\begin{pmatrix}2v_1n_1&v_1n_2+v_2n_1&v_3n_1+v_1n_3\\v_1n_2+v_2n_1&2v_2n_2&v_2n_3+v_3n_2\\v_3n_1+v_1n_3&v_2n_3+v_3n_2&2v_3n_3\end{pmatrix}, \tag{21}$$

where $(\hat{v}\,\hat{b}\,\hat{n})$ is the orthonormal matrix that rotates the coordinate axes.

For the convenience in formulating stress tensor inversion in Section 5, we compose a virtual strain tensor representing the imagined displacement in the direction of $\hat{b}$ on the fault plane (Fig. 2c):

$$\mathbf{E}'=-\frac{\gamma'}{2}\begin{pmatrix}0&0&0\\0&0&1\\0&1&0\end{pmatrix}, \tag{22}$$

which is expressed in the fault coordinate system, where γ' is again the engineering shear strain. In general coordinates:

$$\mathbf{E}'=-\frac{\gamma}{2}\begin{pmatrix}2b_1n_1&b_1n_2+b_2n_1&b_3n_1+b_1n_3\\b_1n_2+b_2n_1&2b_2n_2&b_2n_3+b_3n_2\\b_3n_1+b_1n_3&b_2n_3+b_3n_2&2b_3n_3\end{pmatrix}. \tag{23}$$

4.2. Normalisation of strain tensor

Since the stress tensor inversion does not need the amount of displacement and the volume of rock mass deformed by a fault, we need not specify γ in the observation. Then we normalise it as

$$\gamma=2. \tag{24}$$

On this normalisation, the principal strains are calculated from Eq. (20) to be

$$E_1=1,\quad E_2=0,\quad E_3=-1. \tag{25}$$

The basic invariants are, therefore:

$$J_{\mathrm{I}}(\mathbf{E})\equiv E_1+E_2+E_3=0, \tag{26}$$

$$J_{\mathrm{II}}(\mathbf{E})\equiv -E_2E_3-E_3E_1-E_1E_2=1, \tag{27}$$

$$J_{\mathrm{III}}(\mathbf{E})\equiv E_1E_2E_3=0, \tag{28}$$

where J_{III} is the third invariant (determinant). The same normalisation was assigned to the virtual strain tensor $\mathbf{E}'$, i.e. $\gamma'=2$. Note that a normalised strain tensor $\mathbf{E}$ alone is equivalent to a fault-slip datum.

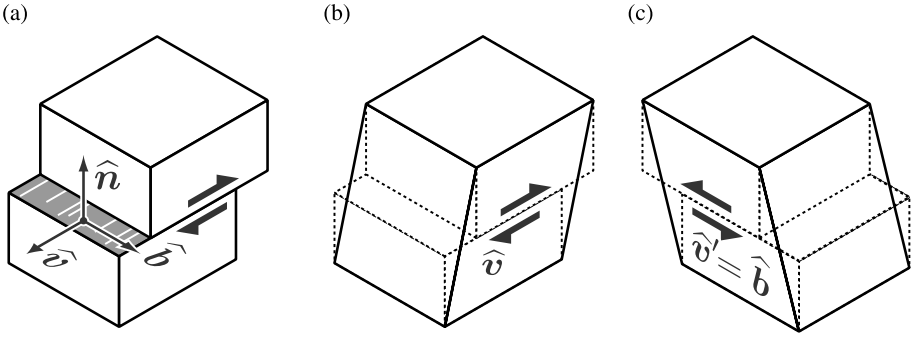

Fig. 2. (a) A fault-slip datum described by the fault normal $\hat{n}$ and the slip direction $\hat{v}$. The vector $\hat{b}$ is on the fault plane at right angles to $\hat{v}$. (b) The simple shear deformation approximating the fault-slip datum in (a). (c) The virtual shear deformation in the direction $\hat{b}$.

The physical meanings of the three normalisations are clear. Eq. (26) represents the constant volume condition, while Eq. (28) implies plane strain. These two are equivalent to the assumption of simple shear. Eq. (27) reflects Eq. (24), reducing the information on the amount of strain.

4.3. ε-vector and ε′-vector

According to our definition of parameter space (Eq. (1)), we can construct a six-dimensional vector from the strain tensor:

$$\begin{aligned}\vec{\varepsilon}^{[6]} \equiv \vec{\mathcal{F}}_6(\mathbf{E}) &= \left(\frac{E_{11}}{\sqrt{2}}, \frac{E_{22}}{\sqrt{2}}, \frac{E_{33}}{\sqrt{2}}, E_{23}, E_{31}, E_{12}\right)^{\mathrm{T}} \\ &= -\Big(\sqrt{2}v_1n_1, \sqrt{2}v_2n_2, \sqrt{2}v_2n_2, \\ &\quad v_2n_3 + v_3n_2, v_3n_1 + v_1n_3, v_1n_2 + v_2n_1\Big)^{\mathrm{T}}, \end{aligned} \tag{29}$$

which we named 'ε-vector'. Similarly, the virtual strain tensor is mapped into

$$\begin{aligned}\vec{\varepsilon}'^{[6]} \equiv \vec{\mathcal{F}}_6(\mathbf{E}') &= \left(\frac{E'_{11}}{\sqrt{2}}, \frac{E'_{22}}{\sqrt{2}}, \frac{E'_{33}}{\sqrt{2}}, E'_{23}, E'_{31}, E'_{12}\right)^{\mathrm{T}} \\ &= -\Big(\sqrt{2}b_1n_1, \sqrt{2}b_2n_2, \sqrt{2}b_2n_2, \\ &\quad b_2n_3 + b_3n_2, b_3n_1 + b_1n_3, b_1n_2 + b_2n_1\Big)^{\mathrm{T}}, \end{aligned} \tag{30}$$

which we call 'ε′-vector' in the following.

Since Eqs. (26) and (27) are the same normalisations as Eqs. (2) and (3), ε- and ε′-vectors have the five-dimensional expressions:

$$\begin{aligned}\vec{\varepsilon}^{[5]} \equiv \vec{\mathcal{F}}_5(\mathbf{E}) = \Bigg(&\left(\frac{1}{\sqrt{2}}+\frac{1}{\sqrt{6}}\right)v_1n_1 - \left(\frac{1}{\sqrt{2}}+\frac{1}{\sqrt{6}}\right)v_2n_2 - \sqrt{\frac{2}{3}}v_3n_3, \\ &-\left(\frac{1}{\sqrt{2}}-\frac{1}{\sqrt{6}}\right)v_1n_1 + \left(\frac{1}{\sqrt{2}}+\frac{1}{\sqrt{6}}\right)v_2n_2 - \sqrt{\frac{2}{3}}v_3n_3, \\ &-v_2n_3 - v_3n_2, -v_3n_1 - v_1n_3, -v_1n_2 - v_2n_1\Bigg)^{\mathrm{T}}, \end{aligned} \tag{31}$$

$$\begin{aligned}\vec{\varepsilon}'^{[5]} \equiv \vec{\mathcal{F}}_5(\mathbf{E}') = \Bigg(&\left(\frac{1}{\sqrt{2}}+\frac{1}{\sqrt{6}}\right)b_1n_1 - \left(\frac{1}{\sqrt{2}}+\frac{1}{\sqrt{6}}\right)b_2n_2 - \sqrt{\frac{2}{3}}b_3n_3, \\ &-\left(\frac{1}{\sqrt{2}}-\frac{1}{\sqrt{6}}\right)b_1n_1 + \left(\frac{1}{\sqrt{2}}+\frac{1}{\sqrt{6}}\right)b_2n_2 - \sqrt{\frac{2}{3}}b_3n_3, \\ &-b_2n_3 - b_3n_2, -b_3n_1 - b_1n_3, -b_1n_2 - b_2n_1\Bigg)^{\mathrm{T}}, \end{aligned} \tag{32}$$

Their common existence region is the five-dimensional unit sphere S_5:

$$\left|\vec{\varepsilon}^{[5]}\right| = 1, \quad \left|\vec{\varepsilon}'^{[5]}\right| = 1. \tag{33}$$

Evaluated in the fault coordinate system (Eqs. (20) and (22)), the vectors $\vec{\varepsilon}^{[6]}$ and $\vec{\varepsilon}'^{[6]}$ are perpendicular to each other:

$$\begin{aligned}\vec{\varepsilon}^{[6]} \cdot \vec{\varepsilon}'^{[6]} &= \frac{1}{2}\left(E_{11}E'_{11} + E_{22}E'_{22} + E_{33}E'_{33}\right) + E_{23}E'_{23} \\ &\quad + E_{31}E'_{31} + E_{12}E'_{12} \\ &= 0. \end{aligned} \tag{34}$$

Since the distance in the parameter space is an invariant of the difference tensor (Section 2.3), the scalar product, which is the cosine of the angular distance between two unit vectors, is independent of reference frame in physical space. Therefore, Eq. (34) is valid for any coordinate system.

5. Stress tensor inversion in parameter space

5.1. The Wallace–Bott hypothesis

Recent inversion methods are based on the Wallace–Bott hypothesis (Wallace, 1951; Bott, 1959), which states that a fault slips in the direction of resolved shear stress exerted on the fault surface (Fig. 3). The condition for a single fault is formulated as

$$\hat{v} = -\tau/|\tau|, \tag{35}$$

where $\boldsymbol{\tau}$ is the resolved shear stress, which is obtained by projecting the traction vector $\boldsymbol{t}$ onto the fault plane. Cauchy's formula, $t = \mathbf{S}\hat{n}$, gives the traction vector from an assumed stress tensor $\mathbf{S}$. An optimal stress tensor is determined essentially by minimising the angular misfits between observed slip directions and theoretical ones given by Eq. (35).

The reduction of the determinable variables of the stress tensor (Section 3.1) is ascribed to the Wallace–Bott hypothesis. We cannot distinguish an arbitrary stress tensor $\mathbf{S}$ and its linear combination $(\alpha\mathbf{S} - \beta\mathbf{I})$, where α and β are arbitrary real numbers, since they give the same direction of shear stress on any fault surfaces (Etchecopar et al., 1981; Angelier, 1984). The parameter α specifies the magnitude of confining pressure that can be considered as a function of the depth of faulting,

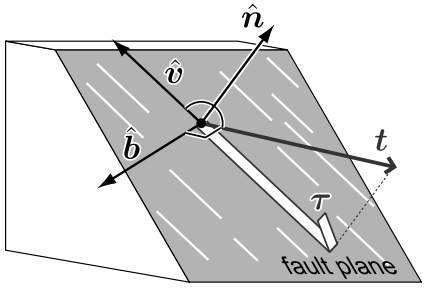

Fig. 3. Explanation for the Wallace–Bott hypothesis. Unit vectors $\hat{n}$, $\hat{v}$ and $\hat{b}$ are the same as those in Fig. 2. The vector $\boldsymbol{t}$ is the traction exerted on the footwall block. The projection of $\boldsymbol{t}$ onto the fault surface gives the shear stress $\boldsymbol{\tau}$. The hypothesis states that $\hat{v}$ and $\boldsymbol{\tau}$ point in the opposite direction, i.e. $\boldsymbol{t}$ should make an obtuse angle with $\hat{v}$ and be perpendicular to $\hat{b}$.

while β corresponds to the pore fluid pressure. Conversely, we need not worry about these parameters and can freely choose two normalisations.

5.2. Wallace–Bott hypothesis in parameter space

The Wallace–Bott hypothesis specifies possible stress tensors required to activate a given fault. Fry (2001) has described the admissible region of σ-vector in his σ-space. However, since the discussion was generalised to deal with magnitudes of stress, he did not employ the normalisations of stress tensor. This subsection introduces the admissible region of normalised σ-vector from the viewpoint of energy balance.

When a fault is activated, the work done on the rock mass by the external tectonic stress is

$$\begin{aligned} W &\equiv \frac{1}{2}\mathbf{E}:\mathbf{S} = \frac{1}{2}\sum_{i,j=1}^{3} E_{ij}S_{ij} \\ &= \frac{1}{2}\left(E_{11}S_{11} + E_{22}S_{22} + E_{33}S_{33}\right) + E_{23}S_{23} + E_{31}S_{31} \\ &\quad + E_{12}S_{12} \\ &= \vec{\varepsilon}^{[6]}\cdot\vec{\sigma}^{[6]}. \end{aligned} \tag{36}$$

TheWallace–Bott hypothesis naturally requires the energy dissipation through the faulting to be positive:

$$W = \vec{\varepsilon}^{[6]}\cdot\vec{\sigma}^{[6]} > 0. \tag{37}$$

On the other hand, the virtual work related to the virtual strain tensor $\mathbf{E}'$ (Section 4.1) should be zero, because the exerted traction vector $\boldsymbol{t}$ is required to be perpendicular to the imagined slip direction $\hat{b}$ (Figs. 2c and 3). Accordingly:

$$W' \equiv \frac{1}{2}\mathbf{E}':\mathbf{S} = \vec{\varepsilon}'^{[6]}\cdot\vec{\sigma}^{[6]} = 0. \tag{38}$$

Eqs. (37) and (38) are equivalent to the Wallace–Bott hypothesis (Eq. (35)), which we can verify from a kinematic viewpoint. Following Fry (2001), we divided the hypothesis into two parts as is visualised in Fig. 3. Firstly, $\boldsymbol{t}$ and $\hat{v}$ should meet at an obtuse angle to be concordant with observed shear sense. Secondly, $\boldsymbol{t}$ and $\hat{b}$ should be perpendicular to each other to make the shear stress $\boldsymbol{\tau}$ parallel to $\hat{v}$. These conditions are formulated as

$$\hat{v}\cdot t = \hat{v}\cdot S\hat{n} = \sum_{i,j=1}^{3} v_i S_{ij} n_j = -\vec{\varepsilon}^{[6]}\cdot\vec{\sigma}^{[6]} < 0, \tag{39}$$

$$\hat{b}\cdot t = \hat{b}\cdot\mathbf{S}\hat{n} = \sum_{i,j=1}^{3} b_i S_{ij} n_j = -\vec{\varepsilon}'^{[6]}\cdot\vec{\sigma}^{[6]} = 0, \tag{40}$$

which are identical to Eqs. (37) and (38), respectively.

In the following equations, the superscript showing the dimension '[5]' is omitted, namely, $\vec{\sigma} \equiv \vec{\mathcal{F}}_5(\mathbf{S})$, $\vec{\varepsilon} \equiv \vec{\mathcal{F}}_5(\mathbf{E})$ and $\vec{\varepsilon}' \equiv \vec{\mathcal{F}}_5(\mathbf{E}')$. Noting Eq. (9), we can now rewrite the Wallace–Bott hypothesis from Eqs. (16), (33), (34), (37) and (38) as

$$\vec{\varepsilon}\cdot\vec{\sigma} > 0, \tag{41}$$

$$\vec{\varepsilon}'\cdot\vec{\sigma} = 0, \tag{42}$$

where

$$|\vec{\sigma}| = |\vec{\varepsilon}| = |\vec{\varepsilon}'| = 1, \tag{43}$$

$$\vec{\varepsilon}\cdot\vec{\varepsilon}' = 0. \tag{44}$$

Eqs. (41) and (42) have similar forms to those proposed by Fry (2001), while the simple features of Eqs. (43) and (44) are available uniquely in the present formulation.

The σ-vector is required to make an acute angle with the ε-vector and to be perpendicular to the ε'-vector (Fig. 4). On the five-dimensional unit sphere S_5, the σ-vector $\vec{\sigma}$ should be in the hemisphere of which pole is $\vec{\varepsilon}$ and on the great circle normal to $\vec{\varepsilon}'$. The intersection between the hemisphere and the great circle is half a great circle, which has an expanse of three dimensions. Consequently, a fault-slip datum specifies its own great semicircle on S_5 and constrains the σ-vector on it based on the Wallace–Bott hypothesis. This simplified admissible region of σ-vector is an equivalent of McKenzie's (1969) solution described by principal orientations and stress ratios.

5.3. Angular misfit in parameter space

For the stress tensor inversion techniques, the angular misfit between the directions of observed slip and resolved shear stress is an essential parameter used as the objective function to be minimised. Our parameter space involves the angular misfit in its geometry. Fig. 5a shows that the angular misfit is

$$\Delta = tan^{-1}\left(-\frac{|\hat{b}\cdot t|}{\hat{v}\cdot t}\right) \quad (0^\circ \le \Delta \le 180^\circ). \tag{45}$$

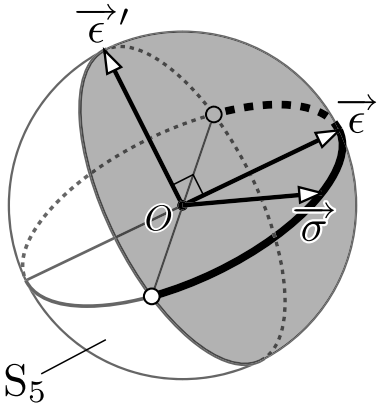

Fig. 4. Schematic figure showing the constraint on the stress tensor from a single fault. The vectors $\vec{\sigma}$, $\vec{\varepsilon}$ and $\vec{\varepsilon}'$ on the five-dimensional unit sphere S_5 represent σ-, ε- and ε'-vectors, respectively. The Wallace–Bott hypothesis restricts $\vec{\sigma}$ on the surface of the hemisphere of which pole is $\vec{\varepsilon}$ (shaded region) and on the great circle perpendicular to $\vec{\varepsilon}'$. Consequently, $\vec{\sigma}$ should be on the half great circle shown by the bold line. Note that the great semicircle actually has an expanse of three dimensions.

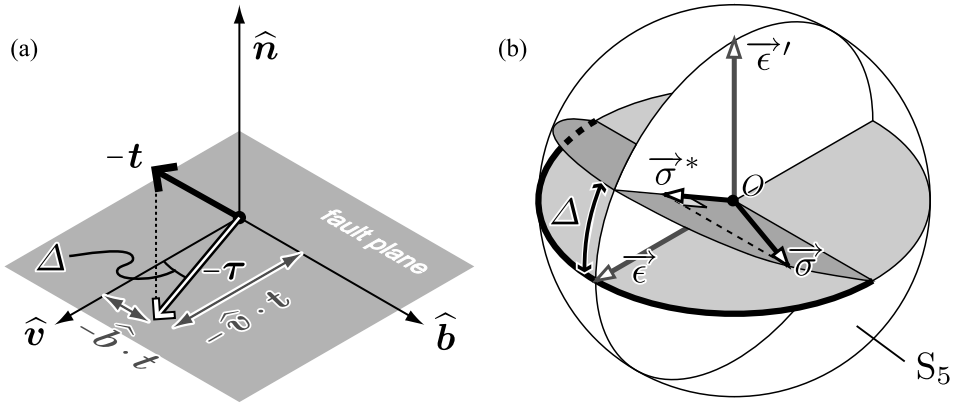

Fig. 5. (a) Angular misfit in physical space. All vectors are the same as those in Figs. 2 and 3. Given a reduced stress tensor, the angular misfit Δ is the angle between $\hat{v}$ and $-\boldsymbol{\tau}$ (see Eq. (35)), which can be rewritten using the direction cosines of the traction vector $\boldsymbol{t}$ for $\hat{b}$ and $\hat{v}$. (b) Angular misfit in the parameter space. A fault-slip datum is represented by ε-vector $\vec{\varepsilon}$ and ε'-vector $\vec{\varepsilon}'$. When a σ-vector $\vec{\sigma}$ is orthogonally projected onto $\vec{\varepsilon}-\vec{\varepsilon}'$ plane to be $\vec{\sigma}^*$, the angular misfit Δ is the angle between $\vec{\varepsilon}$ and $\vec{\sigma}^*$. The angle can be interpreted as the misfit of $\vec{\sigma}$ to the constraint of the great semicircle specified by the fault (bold line). See text for derivation.

Combining Eqs. (39) and (40), we can rewrite Eq. (45) as

$$\Delta = \tan^{-1}\left(\frac{|\vec{\varepsilon}'\cdot\vec{\sigma}|}{\vec{\varepsilon}\cdot\vec{\sigma}}\right) \quad (0^\circ \le \Delta \le 180^\circ). \tag{46}$$

When we take ε- and ε'-vectors as coordinate axes in the parameter space, the scalar products in Eq. (46) are direction cosines of $\vec{\sigma}$ for the two axes. Let $\vec{\sigma}^*$ be the orthogonal projection of $\vec{\sigma}$ onto the two-dimensional $\vec{\varepsilon}-\vec{\varepsilon}'$ plane. Then, the angular misfit Δ is equivalent to the angle between $\vec{\varepsilon}$ and $\vec{\sigma}^*$ (Fig. 5b).

The angular misfit straightforwardly evaluates the deviation of assumed σ-vector from the admissible region of the great semicircle (Figs. 4 and 5b). This geometric interpretation theoretically supports the minimisation of angular misfits in the classical inversion techniques and shows the affinity of our parameter space with the physical space.

5.4. Inversion as an eigenproblem

The inequality (Eq. (41)) and the equality (Eq. (42)) show the non-linear and linear relationships between observable fault parameters and unknown variables of reduced stress tensor, respectively. The stress tensor inversion can be geometrically solved based on the linear aspect. When we have N fault-slip data, N ε'-vectors are constructed as points on S_5. To satisfy the orthogonal condition (Eq. (42)), the optimal orientation of σ-vector is given as the pole of the great circle fitted to the ε'-vectors (Fig. 6).

The fitting is achieved by solving an eigenproblem for the moment of inertia tensor of ε'-vectors (Fry, 1999; Shan et al., 2003):

$$\mathbf{P} = \sum_{i=1}^{N} [\vec{\varepsilon}'^{(i)}][\vec{\varepsilon}'^{(i)}]^{\mathrm{T}}, \tag{47}$$

where $\vec{\varepsilon}'^{(i)}$ is ε'-vector of ith datum. The 5×5 matrix $\mathbf{P}$ is an orientation matrix (e.g. Fisher et al., 1987, p. 33) extended to five dimensions. Since the length of a source vector works as a weight factor in its direction, all ε'-vectors must have unit lengths, which is satisfied by the present formulation. The eigenvector for the minimum eigenvalue gives the optimal orientation of σ-vector. If we compose the orientation matrix from the six-dimensional expressions of ε'-vectors, the resultant 6×6 orientation matrix has a zero eigenvalue for a eigenvector parallel to $\vec{\pi}$ because of the first normalisation (Eq. (2)). In this case, the eigenvector for the second smallest eigenvalue is the optimal solution (Fry, 1999).

We have to choose a pole from two intersection points between S_5 and the line parallel to the eigenvector (Fig. 6). This choice of sign of $\vec{\sigma}$ is the non-linear part of inversion and is made according to the constraints of shear senses (Eq. (41)). If the fault-slip data is homogeneous, namely all faults were activated by a single stress, one of the poles can satisfy all conditions of observed N shear senses, while the other cannot at all.

The above method is called the 'eigenvector method' in the following discussions. Although this method instantly gives the optimal solution, it is not applicable to heterogeneous fault-slip data recording multiple stress states. First of all, ε'-vectors of such a dataset do not lie on a single great circle. Second, the conditions of shear senses will not be satisfied simultaneously.

As a special case of the eigenvector method, suppose that there are just four fault-slip data observed. If their ε'-vectors

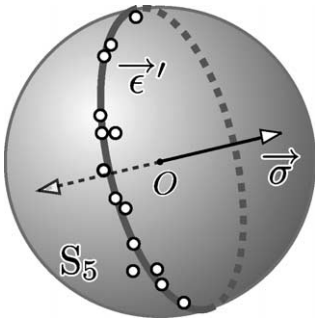

Fig. 6. Schematic figure showing the principle of eigenvector method of stress tensor inversion. The vectors $\vec{\varepsilon}'$ and $\vec{\sigma}$ represent ε'- and σ-vectors, respectively. $\vec{\sigma}$ can be determined as the pole of the great circle that is fitted to the ε'-vectors. The conditions of shear senses constrain the polarity of $\vec{\sigma}$.

are linearly independent, the inversion becomes an even-determined problem, since four vectors are just necessary to constrain a four-dimensional great circle on the five-dimensional sphere. In this case, the optimal stress tensor completely explains the slip orientations. The σ-vector can be calculated as a five-dimensional vector product of the four ε'-vectors. Nevertheless, the constraints of shear senses are again ignored in this method and, hence, they must be checked separately.

6. Test of formulation

6.1. Bias on distribution

The distributions of the vectors in the parameter space have essential roles in the stress estimation. However, as is shown below, the conventional formulation (Fry, 1999) has some bias on the distribution, while the present one can settle this problem.

A random fault-slip dataset was generated for the test on bias. The fault normals are randomly oriented on the three-dimensional unit sphere and the slip directions are also randomly assigned to the fault planes. The random faults are expected to yield no concentrated region in the distribution of ε'-vectors. Using the present and the conventional formulations, we calculated the six-dimensional orientation matrices (Section 5.4) for 100,000 ε'-vectors.

Table 2 shows the eigenvalues and the eigenvectors. Note that the first three dimensions of eigenvectors are the diagonal components of tensors in physical space and the rest are the off-diagonal ones (Eq. (1)). The smallest eigenvalues of both formulations equal zero and their eigenvectors are parallel to $\vec{\pi}$ because of the normalisation of first invariant. As for the present formulation, the other five eigenvalues have almost the same magnitude, showing the isotropic distribution. No preferred orientation was observed in the eigenvectors. Meanwhile, the conventional formulation resulted in two smaller eigenvalues and three larger ones. The eigenvectors for the smaller two have large diagonal components with negligible off-diagonal components, while those for the larger three conversely have large weights in off-diagonal directions (underlined components in Table 2). This background will incline the optimal solution to have large diagonal components.

The difference between formulations can be geometrically explained. Fig. 7a schematically shows the isotropic distribution of ε'-vectors according to the present formulation. The conventional formulation (Fry, 1999) uses the 'f-pole vector':

$$\vec{p} = (b_1n_1,\ b_2n_2,\ b_3n_3,\ b_2n_3 + b_3n_2,\ b_3n_1 + b_1n_3,\ b_1n_2 + b_2n_1)^{\mathrm{T}}, \tag{48}$$

in the eigenvector method. Except for the sign convention, the difference with our ε'-vector (Eq. (30)) is in the first three components without $\sqrt{2}$ factors. Since the conventional σ-vector also does not have the $\sqrt{2}$ factors, the orthogonal condition between σ- and ε'-vectors is available for f-pole vectors. The lack of the factors results in some contraction of the unit sphere only in the diagonal directions (Fig. 7b). According to Fry (1999), the length of the f-pole vector is normalised to be unity in order to calculate the orientation matrix (Fig. 7c). As a result, the normalised f-pole vectors are concentrated in the off-diagonal directions. The above distortion will lower the accuracy of the optimal solution, while our formulation is free from this problem. Sections 6.2 and 7.4 include the experimental comparison of accuracies between these formulations.

6.2. Independence from coordinate selection

The present parameter space is formulated using invariants of stress and strain tensors. This subsection confirms that the distribution of vectors in the parameter space is independent from the choice of coordinate system in physical space.

Table 2
Eigenvalues and eigenvectors of the orientation matrices for ε'-vectors of 100,000 random faults. The smallest eigenvalue is intrinsically zero owing to the normalisation. The present formulation gives the isotropic distribution, while the conventional formulation makes some anisotropy between the diagonal and off-diagonal directions. The italic values show relatively large components in the eigenvectors

Ranking	Eigenvalue	Eigenvector					
		Diagonal components			Off-diagonal components		
	($\times 10^4$)	x_1	x_2	x_3	x_4	x_5	x_6
Present formulation							
1st	0.0000	0.5774	0.5774	0.5774	0.0000	0.0000	0.0000
2nd	1.9803	0.3022	−0.6384	0.3362	0.3320	−0.3528	0.3917
3rd	1.9947	0.3868	0.1776	−0.5645	0.4162	−0.4806	−0.3100
4th	2.0020	−0.1107	−0.2438	0.3544	−0.3346	−0.4242	−0.7147
5th	2.0088	0.6001	−0.2771	−0.3230	−0.6571	0.1536	0.0579
6th	2.0142	−0.2310	0.3023	−0.0713	−0.4158	−0.6641	0.4861
Conventional formulation							
1st	0.0000	0.5774	0.5774	0.5774	0.0000	0.0000	0.0000
2nd	1.4256	*0.2361*	*−0.7949*	*0.5588*	0.0037	−0.0079	0.0079
3rd	1.4347	*0.7816*	*−0.1863*	*−0.5953*	0.0047	−0.0045	0.0006
4th	2.3711	−0.0069	0.0094	−0.0025	*0.7061*	*−0.4494*	*0.5471*
5th	2.3785	0.0026	−0.0009	−0.0017	*−0.0901*	*0.7094*	*>0.6991*
6th	2.3900	−0.0008	0.0042	−0.0034	*−0.7023*	*−0.5429*	*0.4604*

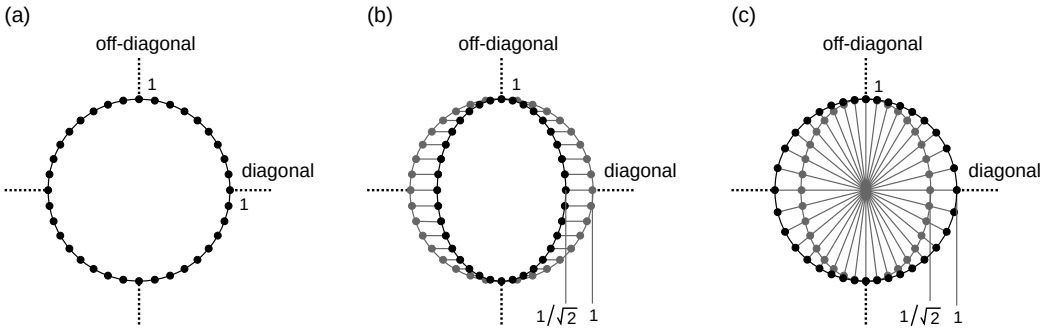

Fig. 7. Schematic figure showing the distribution of ε'-vectors for random fault-slip data in each formulation (Section 6.1). (a) The present definition. The data correspond to isotropically distributed ε'-vectors on the five-dimensional unit sphere (black circles). (b) The conventional ε'-vectors (f-pole vectors) without normalisation (black circles). Gray circles show the corresponding vectors of the present definition. (c) The f-pole vectors (black circles) normalised to have unit lengths. The distribution is distorted from the isotropic one. Grey circles are the vectors before normalisation.

Two coordinate systems were used to analyse an artificial fault-slip dataset including 10,000 faults with randomly oriented fault normals. The coordinate system A has the axes oriented eastward, northward and upward. The coordinate system B has the second and third axes inclined by 45° northward and southward, respectively (Fig. 8). The slip directions were calculated according to an arbitrary chosen stress state with perturbation in rake angles of the directions obeying the normal distribution. We set an extremely large standard deviation of 60° for the perturbation not to simulate natural data, but to make a theoretical consideration. Although the ε'-vectors will be widely distributed on S_5, the optimal solution should converge at the correct solution owing to the large number of faults.

The eigenvector method with our formulation gave exactly the same solutions for the different coordinate systems (Fig. 8a). Their accuracy can be measured by the stress difference to the given stress. The stress differences for the two coordinate systems are equal and sufficiently small ($D=0.0162$). On the other hand, when the conventional formulation is used, the solutions are different (Fig. 8b). The solution from coordinate system A is rather far from the given stress ($D=0.3182$), while that from the coordinate system B has a better accuracy ($D=0.0788$). Note that the principal axes of the conventional solutions are inclined toward each coordinate axis (Fig. 8b) so that the optimal reduced stress tensors have large diagonal components. This kind of bias was predicted in the previous subsection.

Actually, the above-mentioned problem in the conventional formulation is not so serious for practical measurement errors (less than 10°). If the number of faults is not as large (several tens to hundreds), the perturbation from other sources such as spatial and temporal variations of stress field will be more effective than the bias from the formulation.

7. Error estimation in stress tensor inversion

Orife and Lisle (2003) has proposed a measure of concentration of reduced stress tensors. That is the octahedral shear stress of the averaged tensor of them, which was experimentally found to range from 0 to 1. The larger the value becomes, the more concentrated the tensors are. We can now

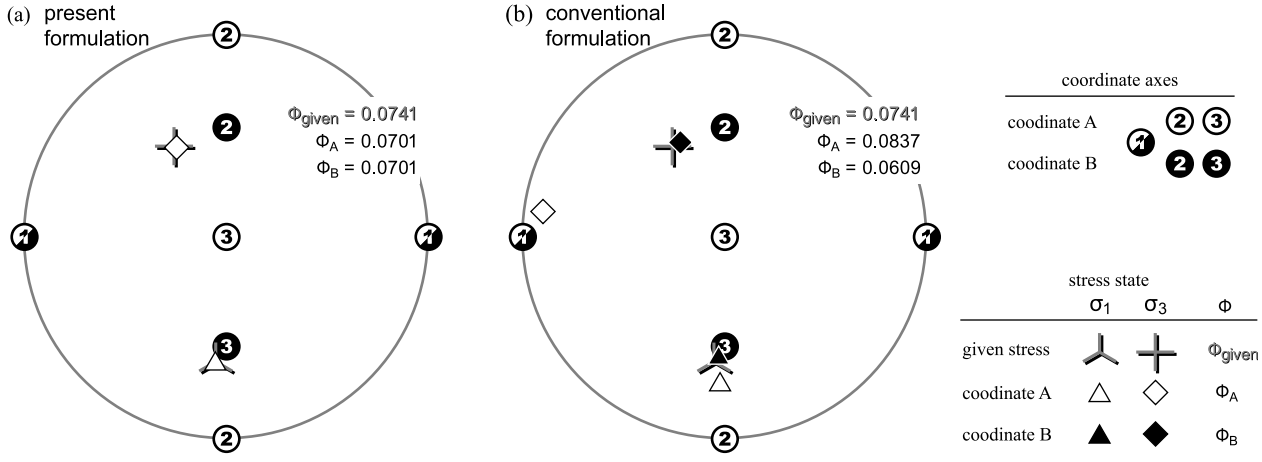

Fig. 8. The resultant stresses from the artificial fault-slip dataset with known solution. The calculations were carried out in two coordinate systems, A and B, of which coordinate axes are indicated by circled numbers. Principal stress axes are shown in the geological convention (σ_1 for the maximum compression as triangles and σ_3 for the minimum compression as diamonds). Open and solid symbols show the axes obtained from coordinate systems A and B, respectively. Stress ratios are noted in the figures. (a) The results from the present formulation. The two coordinate systems gave the same stress state and the symbols are overlapped. (b) The conventional formulation resulted in different solutions between the coordinate systems. See text for the accuracies of solutions (Section 6.2).

interpret their measure as the length of averaged σ-vector (without normalisation onto the unit sphere), since the octahedral shear stress is proportional to the square root of the second invariant (see Eqs. (11) and (C.7)). The mean vector length is a simple and well-used measure of concentration for directional vectors.

However, the above measure is a scalar value. The distribution of σ-vectors, each of which has four degrees of freedom, can be anisotropic in the parameter space. This section provides a straightforward method that can quantify the anisotropy. The method can be used for the error estimation of stress tensor inversion.

7.1. Definition of the confidence region

For the purpose of estimating the variance of reduced stress tensor determined by inversion, the bootstrap method (Efron, 1979) was employed. When there are N fault-slip data, the bootstrap method randomly extracts a fault N times with replacement. Accordingly, an extracted dataset has N faults and probably includes identical ones. Such a generation of dataset is repeated M times and optimal σ-vectors are determined for M datasets by the eigenvector method (Section 5.4).

The best estimate of the σ-vector is given by the mean direction of M solutions:

$$\vec{\mu} = \frac{1}{\rho}\sum_{i=1}^{M}\vec{\sigma}^{(i)}, \tag{49}$$

where $\vec{\sigma}^{(i)}$ is the solution obtained from ith extracted dataset, and ρ is the normalising factor ($\rho = \left|\Sigma\vec{\sigma}^{(i)}\right|$). Each σ-vector has four degrees of freedom and lies on the four-dimensional surface of the unit sphere S_5. Therefore, their variance should be estimated by a four-dimensional covariance matrix. For ith dataset, the difference vector $\vec{\sigma}^{(i)} - \vec{\mu}$ is orthogonally projected onto the four-dimensional plane P^4_μ which is tangent to S_5 at the end point of $\vec{\mu}$ (Fig. 9). The projected vector, which is denoted by $d\vec{\sigma}^{[4](i)}$, gives the four-dimensional covariance matrix as

$$\mathbf{V}^{[4]} = \frac{1}{M}\sum_{i=1}^{M}\left[d\vec{\sigma}^{[4](i)}\right]\left[d\vec{\sigma}^{[4](i)}\right]^{\mathrm{T}}. \tag{50}$$

The projection does not distort the distribution only when the σ-vectors are sufficiently concentrated around the mean direction.

Assuming that the bootstrapped solutions obey the four-dimensional normal distribution, we constructed the confidence ellipsoid as

$$\left[d\vec{\sigma}^{[4]}\right]^{\mathrm{T}}\left[n^2\mathbf{V}^{[4]}\right]^{-1}\left[d\vec{\sigma}^{[4]}\right] = 1. \tag{51}$$

The scalar factor n specifies the confidence level to give the so-called '$n-\sigma$ region', where the symbol σ roughly denotes the standard deviation. Note that $\mathbf{V}^{[4]}$ has four eigenvalues and their square roots (standard deviations) multiplied by n are the principal radii of the confidence ellipsoid. Our formulation gives the radii in the measure of stress difference if they are so small that the distortion caused by the projection is negligible.

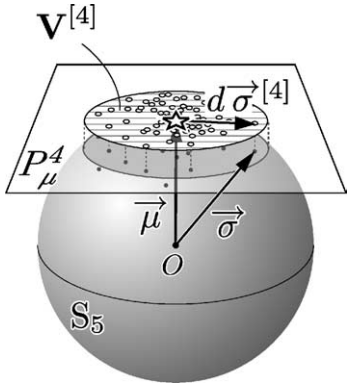

Fig. 9. Geometrical definition of confidence region for reduced stress tensor (analogue of five-dimensional figure). The vectors $\vec{\sigma}$ are the bootstrapped solutions (σ-vectors) of the eigenvector method and $\vec{\mu}$ is their normalised mean vector. The difference vectors $\vec{\sigma} - \vec{\mu}$ are orthogonally projected onto the four-dimensional plane P^4_μ, which is tangent to the unit sphere S_5 at the end point of $\vec{\mu}$. The covariance matrix $\mathbf{V}^{[4]}$ is calculated from the projected vectors $d\vec{\sigma}^{[4]}$. The eigenvalues and eigenvectors of $\mathbf{V}^{[4]}$ are the principal radii and directions of the confidence ellipsoid.

As to the four-dimensional normal distribution, the standard confidence region ($n=1$) corresponds to only 9% of the confidence level (Fig. 10). We shall visualise 59% ($2-\sigma$) or 94% ($3-\sigma$) ellipsoids as confidence regions.

7.2. Visualisation of four-dimensional confidence ellipsoid

The four-dimensional confidence ellipsoid is visualised by using σ-vectors contained in the region. Uniformly distributed 60,000 σ-vectors (Sato and Yamaji, 2006) are used to test whether they are in the ellipsoid or not. The corresponding reduced stress tensors are plotted on the paired stereograms of Yamaji (2000), which can simultaneously show the orientations of σ_1 and σ_3 axes and the stress ratio.

To show examples of visualisation, artificial covariance matrices $\mathbf{V}^{[4]}_{\mathrm{isotropic}}$ and $\mathbf{V}^{[4]}_{\mathrm{anisotropic}}$ were generated. They represent isotropic (spherically symmetric) and anisotropic distributions, respectively. The principal radii of standard

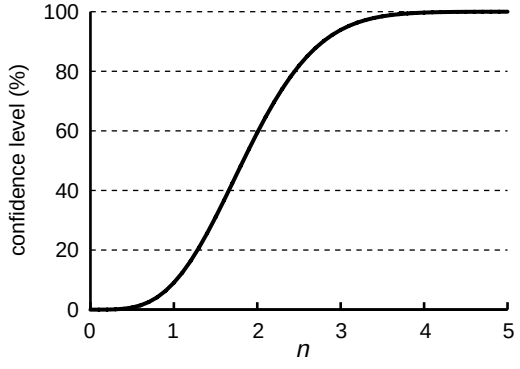

Fig. 10. Confidence level calculated from probability density function of four-dimensional normal distribution. The horizontal axis is the factor n, which specifies the confidence level of $n-\sigma$ confidence ellipsoid. Note that $1-\sigma$ region achieves only a 9% confidence level.

ellipsoids (square roots of eigenvalues) were given as

$$\mathbf{V}^{[4]}_{\text{isotropic}}: \quad (0.1,\ 0.1,\ 0.1,\ 0.1),$$

$$\mathbf{V}^{[4]}_{\text{anisotropic}}: (0.2,\ 0.1,\ 0.1,\ 0.05).$$

Note that two ellipsoids have the same volume, since the products of the four radii are equal. They had a common centre $\vec{\mu}$ that corresponds to the reduced stress tensor of which σ_1 and σ_3 axes are oriented to 180/45 and 000/45, respectively, with a stress ratio of $\Phi = 0.25$ (see Appendix C for the definition of Φ). In what follows, we use the geological sign convention that compression is positive to describe the principal stresses with the symbols σ_1, σ_2 and σ_3.

Fig. 11 shows the visualised variances. A tadpole-like symbol represents a reduced stress tensor (Yamaji, 2000). Orientations of σ_1 axes are plotted as 'heads' (small squares) in each left-hand stereogram. The lengths and directions of attached 'tails' (bars) indicate orientations of σ_3 axes, as if there were small stereograms around the 'heads'. The right-hand stereograms are complementary ones in which the roles of 'heads' and 'tails' are interchanged, i.e. the 'heads' are σ_3 axes and the 'tails' are σ_1 axes. The greyscale colours of tadpoles indicate the values of stress ratios.

The isotropic covariance $\mathbf{V}^{[4]}_{\text{isotropic}}$ resulted in the principal stress axes and the stress ratios, which are symmetrically distributed with respect to the principal stress planes of $\vec{\mu}$ (Fig. 11a and b for 59 and 94% confidence regions, respectively). The lower the stress ratio is (dark colours), the broader the σ_3 axes are scattered on the principal plane normal to the σ_1 axis of $\vec{\mu}$. This observation shows the interdependence between the dispersion of principal orientation and that of stress ratio. The confidence regions of the anisotropic covariance $\mathbf{V}^{[4]}_{\text{anisotropic}}$ are shown in Fig. 11c (59%) and Fig. 11d (94%). They show distorted patterns, compared with the isotropic case.

7.3. Numerical experiment 1

With the bootstrapped inversion method, an artificial fault-slip dataset (Fig. 12a) was analysed to estimate the confidence region of the optimal solution. The dataset includes $N = 20$ faults and their fault planes are randomly oriented. An arbitrarily chosen stress state

$$\sigma_1 - \text{axis}: \quad 154/43, \quad \sigma_3 - \text{axis}: \quad 264/20, \quad \Phi = 0.304$$

was assigned to the faults and theoretical slip directions were calculated according to the Wallace–Bott hypothesis. Angular random errors were imposed on the slip directions, which obeyed the normal distribution with the mean of zero and the standard deviation of 15°. The bootstrap resampling was repeated $M = 200$ times.

All stress tensors output by the eigenvector method are plotted on Fig. 12b. Their mean solution

$$\sigma_1 - \text{axis}: \quad 159/37, \quad \sigma_3 - \text{axis}: \quad 263/19, \quad \Phi = 0.340,$$

is roughly equal to the correct solution, although the perturbation of 15° is large. Fig. 12c shows the 94% confidence

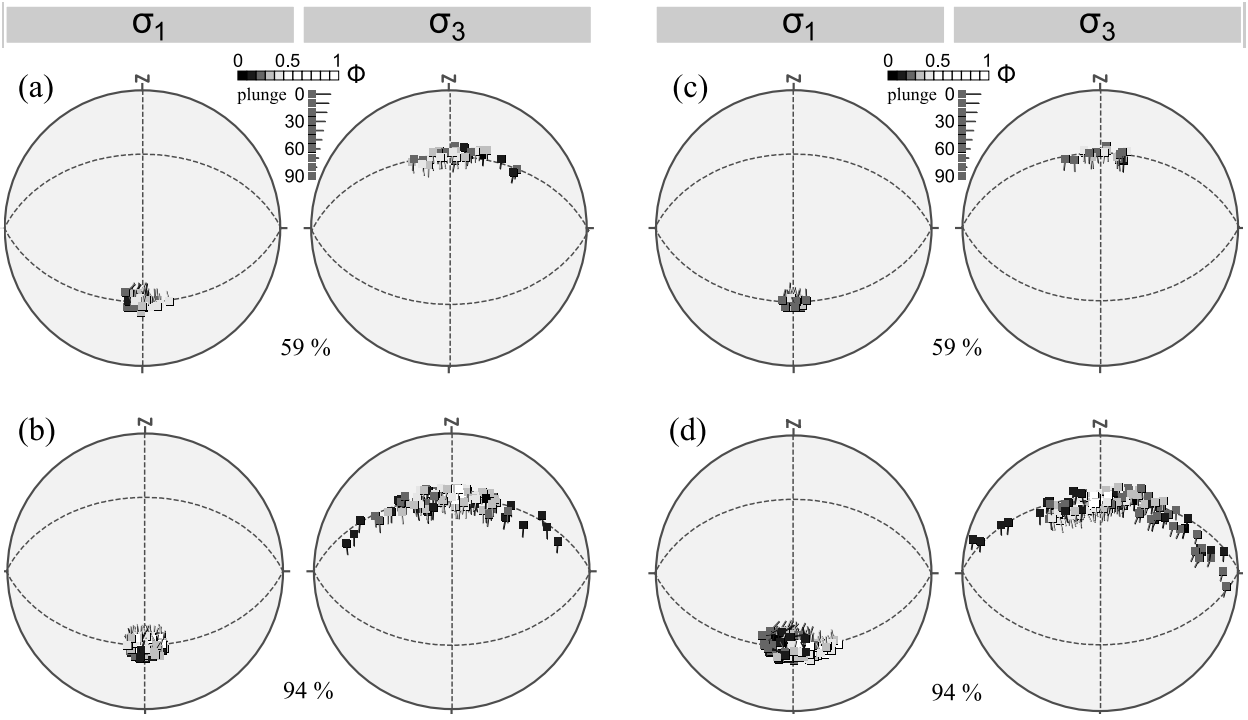

Fig. 11. Paired stereograms visualising the artificial confidence ellipsoids. The given centre of ellipsoid, which is assumed to be the mean σ-vector, is common and its corresponding principal stress planes are shown by broken lines. Figures (a) and (b) show 59 and 94% confidence regions for an isotropic (spherically symmetric) covariance matrix, $\mathbf{V}^{[4]}_{\text{isotropic}}$, while figures (c) and (d) show those for an anisotropic one, $\mathbf{V}^{[4]}_{\text{anisotropic}}$. They were visualised by plotting reduced stress tensors of which σ-vectors are included in the confidence regions. See text for the method of plotting reduced stress tensors.

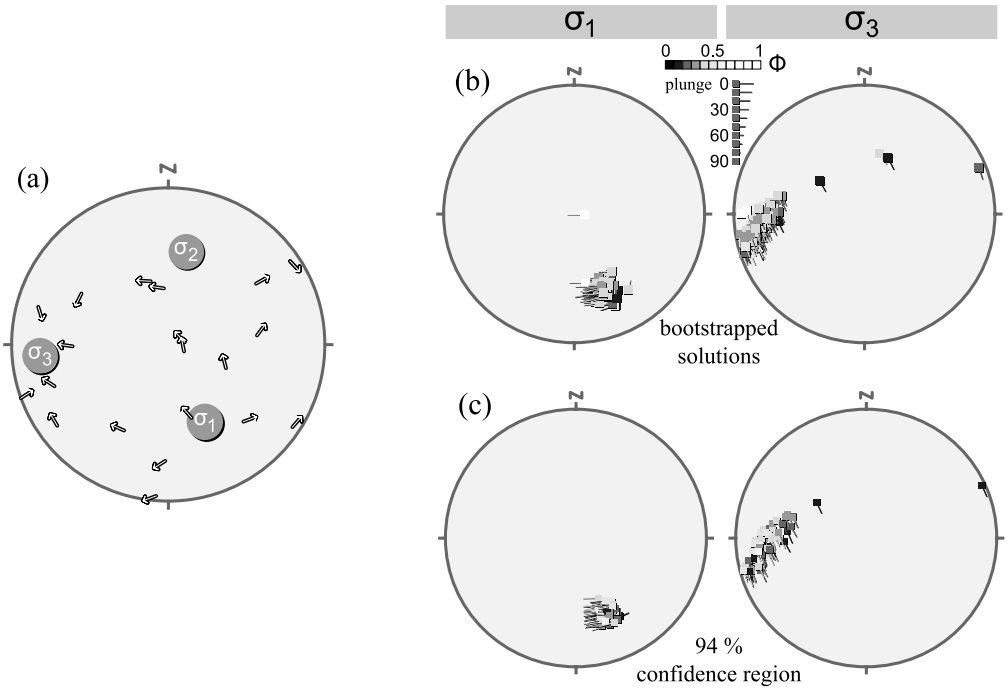

Fig. 12. (a) The perturbed fault-slip data used in the numerical experiment. The data includes 20 faults and is shown by the tangent-lineation diagram (Twiss and Gefell, 1990) with equal-area and lower hemisphere projection. The arrows are plotted in the positions of fault normals. They point to the slip directions of footwall blocks. Each slip direction was perturbed by angular random error with standard deviation of 15°. (b) All solutions generated by the bootstrap iteration ($M=200$). The method of plotting reduced stress tensors is the same as for Fig. 11. (c) The 94% confidence region of the mean solution. The ranges of stress ratios and principal orientations are almost identical to those of (b), supporting our method of quantifying variance.

region of the above mean solution. The standard principal radii (standard deviations) are

$$\mathbf{V}^{[4]}: \quad (0.139, \quad 0.111, \quad 0.083, \quad 0.063).$$

The covariance matrix had some anisotropy that the maximum principal radius was larger than double the minimum one. Note that Fig. 12b and c are almost identical in both orientation and stress ratios, verifying our quantification of variance and the assumption of normal distribution of projected σ-vectors on P^4_μ.

7.4. Numerical experiment 2

Another numerical experiment was carried out to compare the precisions of the conventional formulation (Fry, 1999) and the present one. In the sense of a Monte-Carlo test, we generated 100 homogeneous fault-slip datasets, each including 100 faults with randomly oriented fault planes. The reduced stress tensors were randomly chosen on the unit sphere S_5 for each dataset, and the slip directions were calculated according to the stress. The perturbation was imposed on the slip

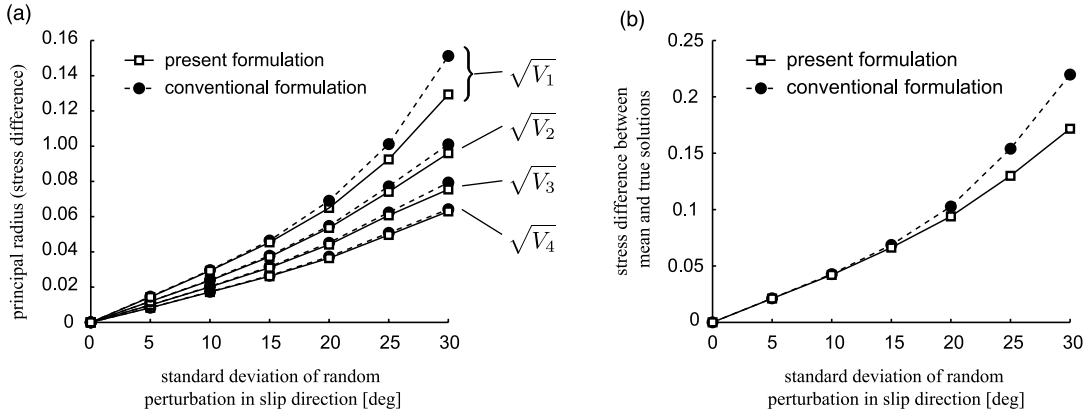

Fig. 13. Results of Monte-Carlo test to compare the present formulation with the conventional one by quantifying the variance and accuracy of deduced stress tensor. The abscissa is the standard deviation of random error on the slip directions. (a) Four principal radii, $\sqrt{V_1}$–$\sqrt{V_4}$, of standard confidence ellipsoid averaged for 100 datasets. The maximum radius ($\sqrt{V_1}$) is larger than double the minimum one ($\sqrt{V_4}$). The present formulation performs relatively smaller confidence region, especially for noisy data. (b) The stress difference between the mean of bootstrapped solutions and the correct solution given artificially. The values are averaged for results from 100 datasets. The present formulation resulted in higher accuracy (smaller stress difference to the correct solution).

directions as random errors of which the standard deviation is varied from 0° (no perturbation) to 30°. The datasets were converted to f-pole vectors (Fry, 1999) or ε'-vectors (this study) and analysed by 200 iterations of the bootstrapped eigenvector method.

The resultant variances are shown by principal radii of standard $(1-\sigma)$ confidence ellipsoids averaged for the 100 cases (Fig. 13a). Both formulations yielded anisotropic variances. The magnitudes of variance are relatively small for our formulation, particularly in the case of large perturbation. To estimate the accuracy of determined stress, the stress differences between mean solutions and given stresses were also measured. Fig. 13b shows the stress differences averaged for 100 cases. Our formulation was found to have higher accuracy in the case of noisy data. This difference between formulations can be attributed to the bias mentioned in Section 6. Since the solution of conventional analysis in each bootstrap iteration has lower accuracy, the precision estimated from 200 iterations is also lowered.

8. Summary

The geometrical interpretation of stress tensor inversion was rearranged to evaluate the difference between stress states by the distance between points in the parameter space. The features of the present formulation are as follows:

1. Fault-slip data are represented by strain tensors.
2. Both stress and strain tensors are normalised only by their basic invariants.
3. The tensors are mapped onto the parameter space with a common rule to be vectors with their end points on the five-dimensional unit sphere.
4. A fault-slip datum constrains the vector representing a stress tensor on a four-dimensional half great circle.
5. The angular misfit between observed slip direction and resolved shear stress corresponds to the deviation angle of the vector representing stress tensor from the half great circle.
6. The Euclidean metric in the parameter space is equivalent to the stress difference.

Features 4 and 5 are particularly important for composing or assessing an inversion method. Based on this geometry, Yamaji et al. (2006) proposed a concise technique to distinguish plural stresses from a heterogeneous dataset. This paper, meanwhile, presented a method for quantifying the variance of deduced stress tensor based on feature 6. In addition, the numerical experiments showed that the modified formulation performs relatively higher precision and accuracy in stress determination than the conventional one. Sato and Yamaji (2006) provide another usage of the metric in generating a set of reduced stress tensors with uniform intervals, which can be used as a search grid to enhance the resolution and the computational efficiency of inversion.

This study entirely depended on the work of Fry (1999, 2001) for σ-space and Orife and Lisle (2003) for the stress difference. Our parameter space is a modified version of σ-space where the stress difference is embedded as metric. Since the equality between the metric and the square root of the second invariant of tensor quantity is valid without the normalisation of magnitudes of stress and strain, the present formulation has a potential application in discussing the mechanics of faulting and the constitutive equations.

Acknowledgements

The authors are grateful to Yehua Shan for his detailed suggestions about the error estimation. Richard Lisle, Norman Fry and the anonymous reviewer are also thanked for their careful and useful comments. This work was supported by Kyoto University Active Geosphere Investigations for the 21st Century Centers of Excellence Program (KAGI21), and by the Japan Society for the Promotion of Science (No. 14540423).

Appendix A. Five-dimensional vector representing deviatoric tensor

If a symmetric tensor $\mathbf{X}$ is deviatoric, its corresponding vector $\vec{x}^{[6]} = \vec{\mathcal{F}}_6(\mathbf{X})$ indicates a point on the plane P^5_π (Eq. (4)). Then a suitable coordinate rotation, which directs a coordinate axis normal to P^5_π, can make a component of $\vec{x}^{[6]}$ zero. We adopted the orthonormal tensor:

$$\mathbf{Q} = \begin{pmatrix} \frac{1}{\sqrt{3}} & \frac{1}{\sqrt{3}} & \frac{1}{\sqrt{3}} & 0 & 0 & 0 \\ -\frac{1}{2}-\frac{1}{2\sqrt{3}} & \frac{1}{2}-\frac{1}{2\sqrt{3}} & \frac{1}{\sqrt{3}} & 0 & 0 & 0 \\ \frac{1}{2}-\frac{1}{2\sqrt{3}} & -\frac{1}{2}-\frac{1}{2\sqrt{3}} & \frac{1}{\sqrt{3}} & 0 & 0 & 0 \\ 0 & 0 & 0 & 1 & 0 & 0 \\ 0 & 0 & 0 & 0 & 1 & 0 \\ 0 & 0 & 0 & 0 & 0 & 1 \end{pmatrix}, \tag{A.1}$$

to obtain a five-dimensional vector $\vec{x}^{[5]}$ as

$$x^{[5]}_{i-1} = \sum_{j=1}^{6} Q_{ij} x^{[6]}_j \quad (\text{for} \quad i = 2, 3, \ldots, 6). \tag{A.2}$$

The first coordinate axis is rotated to be $\vec{\pi} = (\frac{1}{\sqrt{3}}, \frac{1}{\sqrt{3}}, \frac{1}{\sqrt{3}}, 0, 0, 0)^{\mathrm{T}}$ and the component in this direction is truncated. Since the other five axes can be freely oriented, the rotation tensor $\mathbf{Q}$ is not unique. Only the first row of $\mathbf{Q}$ must be $\vec{\pi}$. The five-dimensional expression $\vec{\mathcal{F}}_5(\mathbf{X})$ (Eq. (6)) is the result of the above rotation and truncation.

Appendix B. Metric in parameter space

Given arbitrary symmetric and deviatoric tensors $\mathbf{X}_\mathrm{A}$ and $\mathbf{X}_\mathrm{B}$, the Euclidean distance between corresponding points in the parameter space is evaluated as

$$\left|\vec{\mathcal{F}}_6(\mathbf{X}_A)-\vec{\mathcal{F}}_6(\mathbf{X}_B)\right| = \left|\vec{\mathcal{F}}_6(\mathbf{X}_A-\mathbf{X}_B)\right| = \left|\vec{\mathcal{F}}_6(\mathbf{X}_D)\right|$$
$$= \left[\frac{1}{2}(X_{D11}^2+X_{D22}^2+X_{D33}^2)+X_{D23}^2+X_{D31}^2+X_{D12}^2\right]^{1/2}$$
$$\equiv \sqrt{J_{II}(\mathbf{X}_D)}, \tag{B.1}$$

where $\mathbf{X}_D=\{X_{Dij}\}=\mathbf{X}_A-\mathbf{X}_B$. The first equal sign in Eq. (B.1) is supported by the definition of $\vec{\mathcal{F}}_6$ (Eq. (1)), since the vector subtraction is directly the component-wise tensor subtraction. Note that the difference tensor $\mathbf{X}_D$ as well as $\mathbf{X}_A$ and $\mathbf{X}_B$ is deviatoric, because $J_I(\mathbf{X}_D)=J_I(\mathbf{X}_A)-J_I(\mathbf{X}_B)=0$. Based on Eq. (8), Eq. (B.1) can be rewritten in the five-dimensional expression (Eq. 10).

Appendix C. Principal values of normalised stress tensor

The principal values of reduced stress tensors can be described by the stress ratio:

$$\Phi = (\sigma_2-\sigma_3)/(\sigma_1-\sigma_3), \tag{C.1}$$

where σ_1, σ_2 and σ_3 are the principal stresses ($\sigma_1\geq\sigma_2\geq\sigma_3$, compression being positive). The value of Φ ranges from 0 to 1. The cases $\Phi=0$ and $\Phi=1$ represent stresses of axial compression ($\sigma_1>\sigma_2=\sigma_3$) and axial tension ($\sigma_1=\sigma_2>\sigma_3$), respectively.

In practice, our normalisations (Eq. (12)) can be achieved by giving principal values as

$$\sigma_1=(2-\Phi)/\lambda, \quad \sigma_2=(2\Phi-1)/\lambda, \quad \sigma_3=(-\Phi-1)/\lambda, \tag{C.2}$$

where

$$\lambda=\sqrt{3\Phi^2-3\Phi+3}. \tag{C.3}$$

Substituting Eq. (C.2) into the definitions of first and second invariant, we can confirm the normalisations as follows:

$$J_I(\sigma)=\sigma_1+\sigma_2+\sigma_3=0 \tag{C.4}$$

$$J_{II}(\sigma)=-\sigma_2\sigma_3-\sigma_3\sigma_1-\sigma_1\sigma_2=1. \tag{C.5}$$

Also in the sign convention that tension is positive, we have $J_I(\mathbf{S})=-J_I(\boldsymbol{\sigma})=0$ and $J_{II}(\mathbf{S})=J_{II}(\boldsymbol{\sigma})=1$ since $S_1=-\sigma_3$, $S_2=-\sigma_2$ and $S_3=-\sigma_1$.

The formula of three principal stresses are very similar to those of Orife and Lisle (2003). They adopted the normalisations, $J_I(\boldsymbol{\sigma})=0$ and $\tau_{oct}(\boldsymbol{\sigma})=1$, where τ_{oct} is the octahedral shear stress, a tensor invariant. Their numerators were identical to those of Eq. (C.2) and the denominator was

$$\lambda'=\sqrt{2\Phi^2-2\Phi+2}, \tag{C.6}$$

instead of λ. This similarity comes from the close relationship between τ_{oct} and the second invariant (e.g. Fung, 1965, p. 80):

$$\tau_{oct}=\sqrt{\frac{2}{3}J_{II}}. \tag{C.7}$$

Appendix D. Stress difference

Orife and Lisle (2003) have introduced the stress difference, a very useful measure of difference between reduced stress tensors. Their normalisations were different from ours (Appendix C). In this appendix, an equivalent expression of stress difference is presented.

We distinguish the reduced stress tensors in two conventions by $\boldsymbol{\sigma}^{[oct]}$ (normalised by $J_I=0$ and $\tau_{oct}=1$; Orife and Lisle, 2003) and $\sigma^{[J_{II}]}$ (normalised by $J_I=0$ and $J_{II}=1$; this study). Since the principal values of $\boldsymbol{\sigma}^{[oct]}$ and $\sigma^{[J_{II}]}$ are different by the factor $\sqrt{2/3}$ (Eqs. (C.3) and (C.6)), they are related by

$$\sigma^{[J_{II}]}=\sqrt{\frac{2}{3}}\sigma^{[oct]}. \tag{D.1}$$

Orife and Lisle (2003) have defined the stress difference between two tensors $\boldsymbol{\sigma}_A$ and $\boldsymbol{\sigma}_B$ as

$$D(\sigma_A,\sigma_B)\equiv\tau_{oct}\left(\sigma_D^{\langle oct\rangle}\right), \tag{D.2}$$

where $\sigma_D^{\langle oct\rangle}=\sigma_A^{[oct]}-\sigma_B^{[oct]}$. Note that the octahedral shear stresses of $\sigma_A^{[oct]}$ and $\sigma_B^{[oct]}$ have been normalised to be unity, while that of $\sigma_D^{\langle oct\rangle}$ is the stress difference itself. Using Eqs. (C.7) and (D.1), we can rewrite the definition as

$$D(\sigma_A,\sigma_B)=\left[\left(\frac{2}{3}\right)J_{II}\left(\sigma_A^{[oct]}-\sigma_B^{[oct]}\right)\right]^{\frac{1}{2}}$$
$$=\left[J_{II}\left(\sqrt{\frac{2}{3}}\sigma_A^{[oct]}-\sqrt{\frac{2}{3}}\sigma_B^{[oct]}\right)\right]^{\frac{1}{2}}$$
$$=\left[J_{II}\left(\sigma_A^{[J_{II}]}-\sigma_B^{[J_{II}]}\right)\right]^{\frac{1}{2}}=\sqrt{J_{II}\left(\sigma_D^{\langle J_{II}\rangle}\right)}, \tag{D.3}$$

where $\sigma_D^{\langle J_{II}\rangle}=\sigma_A^{[J_{II}]}-\sigma_B^{[J_{II}]}$, and the equation:

$$aJ_{II}(\sigma)=J_{II}(\sqrt{a}\sigma) \quad (^\forall a\geq 0),$$

was employed since the second invariant is a quadratic quantity. Owing to $J_{II}(\mathbf{S})=J_{II}(\boldsymbol{\sigma})$, Eq. (D.3) is applicable to the alternative sign convention that tension is positive. Consequently, the stress difference corresponds to the square root of the second invariant of the difference tensor based on our normalisations (Eq. (17)).

References

Albarello, D., 2000. A resampling approach to test stress-field uniformity from fault data. Geophysical Journal International 140, 535–542.

Angelier, J., 1979. Determination of the mean principal directions of stresses for a given fault population. Tectonophysics 56, T17–T26.

Angelier, J., 1984. Tectonic analysis of fault slip data sets. Journal of Geophysical Research 89, 5835–5848.

Bott, M.H.P., 1959. The mechanics of oblique slip faulting. Geological Magazine 96, 109–117.

Carey, M.E., Brunier, M.B., 1974. Analyse théorique et numérique d'un modèle mécanique élémentaire appliqué à l'étude d'une population de failles. Compte Rendus de l'Académie des Sciences 279, 891–894.

Choi, P.Y., Angelier, J., Souffache, B., 1996. Distribution of angular misfits in fault-slip data. Journal of Structural Geology 18, 1353–1367.

Efron, B., 1979. The 1977 Rietz Lecture—Bootstrap methods: another look at the Jackknife. Annals of Statistics 7, 1–26.

Etchecopar, A., Vasseur, G., Daignieres, M., 1981. An inverse problem in microtectonics for the determination of stress tensors from fault striation analysis. Journal of Structural Geology 3, 51–65.

Fisher, N.I., Lewis, T., Embleton, B.J.J., 1987. Statistical Analysis of Spherical Data. Cambridge University Press, Cambridge.

Fry, N., 1999. Striated faults: visual appreciation of their constraint on possible paleostress tensors. Journal of Structural Geology 21, 7–21.

Fry, N., 2001. Stress space: striated faults, deformation twins, and their constraints on paleostress. Journal of Structural Geology 23, 1–9.

Fung, Y.C., 1965. Foundations of Solid Mechanics. Prentice Hall, Englewood Cliffs, New Jersey.

Gephart, J.W., Forsyth, D.W., 1984. An improved method for determining the regional stress tensor using earthquake focal mechanism data—application to the San-Fernando earthquake sequence. Journal of Geophysical Research 89, 9305–9320.

Khan, A.S., Huang, S., 1995. Continuum Theory of Plasticity. John Wiley & Sons, New York.

Levitas, V.I., Preston, D.L., 2002. Three-dimensional Landau theory for multivariant stress-induced martensitic phase transformations, II. Multivariant phase transformations and stress space analysis. Physical Review B 66 (134206), 1–15.

McKenzie, D.P., 1969. The relation between fault plane solutions for earthquakes and the directions of the principal stresses. Bulletin of the Seismological Society of America 59, 591–601.

Nemcok, M., Lisle, R.J., 1995. A stress inversion procedure for polyphase fault/slip data sets. Journal of Structural Geology 17, 1445–1453.

Orife, T., Lisle, R.J., 2003. Numerical processing of palaeostress results. Journal of Structural Geology 25, 949–957.

Sato, K., Yamaji, A., 2006. Uniform distribution of points on a hypersphere for improving the resolution of stress tensor inversion. Journal of Structural Geology, this special issue, doi.:10.1016/j.jsg.2006.03.007

Shan, Y.H., Suen, H.B., Lin, G., 2003. Separation of polyphase fault/slip data: an objective-function algorithm based on hard division. Journal of Structural Geology 25, 829–840.

Simón-Gómez, J.L., 1986. Analysis of a gradual change in stress regime (example from the eastern Iberian chain, Spain). Tectonophysics 124, 37–53.

Takahashi, H., Ito, K., Goya, M., 1990. Directional dependence of plastic strain-rate vector on stress-rate vector: numerical experiments based on the Lin's polycrystal model. International Journal of Plasticity 6, 615–632.

Twiss, R.J., Gefell, M.J., 1990. Curved slickenfibers: a new brittle shear sense indicator with application to a sheared serpentinite. Journal of Structural Geology 12, 471–481.

Wallace, R.E., 1951. Geometry of shearing stress and relation to faulting. Journal of Geology 59, 118–130.

Xu, P.L., 2004. Determination of regional stress tensors from fault-slip data. Geophysical Journal International 157, 1316–1330.

Yamaji, A., 2000. The multiple inverse method: a new technique to separate stresses from heterogeneous fault-slip data. Journal of Structural Geology 22, 441–452.

Yamaji, A., 2003. Are the solutions of stress inversion correct? Visualization of their reliability and the separation of stresses from heterogeneous fault-slip data. Journal of Structural Geology 25, 241–252.

Yamaji, A., Tomita, S., Otsubo, M., 2005. Bedding tilt test for paleostress analysis. Journal of Structural Geology 27, 161–170.

Yamaji, A., Otsubo, M., Sato, K., 2006. Paleostress analysis using the Hough transform for separating stresses from heterogeneous fault-slip data. Journal of Structural Geology, this special issue, doi.:10.1016/j.jsg.2006.03.016